A multiscale investigation into the effect of grain size on void evolution and fracture of metallic materials: experiments and crystal plasticity modeling

Xiaoqing Shang [a], Haiming Zhang [a, *], Zhenshan Cui [a, **], M.W. Fu [b, c], Jianbo Shao [d]

[a] Institute of Forming Technology & Equipment, Shanghai Jiao Tong University, 1954 Huashan Road, Shanghai 200030, P.R. China

[b] Department of Mechanical Engineering, The Hong Kong Polytechnic University, Hung Hom, Kowloon, Hong Kong

[c] PolyU Shenzhen Research Institute, No. 18 Yuexing Road, Nanshan District, Shenzhen, P.R. China

[d] School of Materials Science and Engineering, Central South University, Changsha 410083, P.R. China

Abstract

The effect of grain structure on micro-void evolution and further macroscopic fracture was studied through physical experiment and crystal plasticity (CP) modeling. A series of experiments together with the full-field crystal plasticity finite element (CPFE) simulations were conducted to examine the growth and coalescence of voids in an austenite steel 316LN subjected to uniaxial tension. Different morphologies of the fracture surface are observed in experiments for samples with different grain sizes, indicating a change of void behaviors with the grain size. CPFE simulation for representative volume elements (RVEs) with different grain sizes was conducted, and the results show that the deformation and size of void become more heterogeneous as the grain size is increased. In addition, the growth of void is figured out to be more related to the non-uniform deformation than to the non-uniform stress distribution. With the large localized strain, the void grows more obviously. The distribution of void size is quantitatively analyzed and the Gaussian function is found to be able to represent the distribution of major void diameter in a certain grain size condition. An extended model representing the effect of grain size was thus proposed for predicting the

growth of void in polycrystalline metals. Furthermore, the relationship between ductility and grain size was explored. In the fine grain scenario where the deformation heterogeneity is only microscopical, the ductility fluctuates with grain size. However, when the grain size is large enough for inducing macroscopic deformation concentration, the ductility decreases severely as ductile fracture forms in the deformation localization zone at a smaller strain. This study advances the comprehensive understanding of the micro-mechanics of ductile fracture for metallic materials and the relation between microstructure and the macroscopic fracture behavior.

Keywords: Grain size; Deformation heterogeneity; Void growth and coalescence; Crystal plasticity; Damage and fracture.

Corresponding authors:

* Haiming Zhang;

E-mail: hm.zhang@sjtu.edu.cn

** Zhenshan Cui;

E-mail: cuizs@sjtu.edu.cn

1. Introduction

Ductile fracture critically affects the formability of metals in industrial operations and the service performance of products in different applications. Ductile fracture is a multiscale issue and the characterization of which at different length scales is shown in Fig. 1. At macroscopic scale, the ductility of materials is usually measured by elongation or fracture strain, and identified to be affected by stress state (Li et al., 2011; Lou et al., 2012; Ueda et al., 2014), temperature, strain rate, and et al (Khan and Liu, 2012; Novella et al., 2015; Shang et al., 2018). At microscopic scale, voids nucleate with the debonding or cracking of inclusions from the base matrix, and the growth and coalescence of voids eventually give rise to the macroscopic fracture. Generally, the size of void is in the same length scale of grains, and the grain structure, including grain size and mixed crystals, and their evolution, such as the dynamic recrystallization, significantly affect the evolution of voids. The microstructure affected void behavior is manifested as the change of formability at macroscale (Lou et al., 2017; Yang et al., 2018; Yang et al., 2019). Therefore, figuring out the relationship between microstructure, void behavior and macro-fracture is crucial for establishing an in-depth understanding and insight into the ductile fracture behavior of polycrystalline metals.

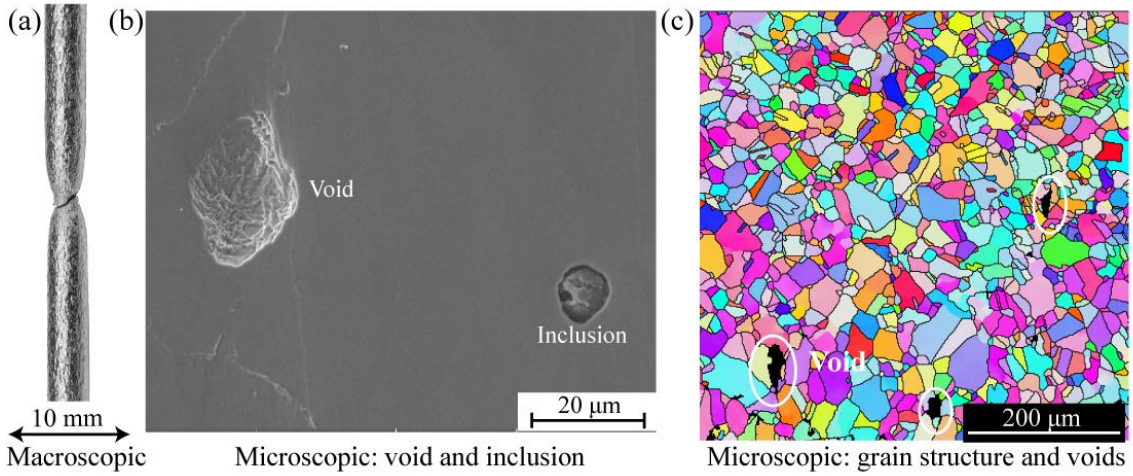

Fig. 1. Characterization of ductile fracture at macroscale and microscale: (a) macroscopic fracture, (b) void and inclusion observed via scanning electron microscopy (SEM), and (c) electron backscatter diffraction (EBSD) image of the microstructure containing voids.

Among many efforts in studying of ductile fracture, experimental investigations into the void behavior were primarily conducted with the aid of various measurement methods. Noell et al. (2017) examined the void nucleation by employing the techniques of EBSD, transmission Kikuchi diffraction, and transmission electron microscopy (TEM), and pointed out that for pure metals, voids generally nucleate at grain boundaries and the triple-junction grain boundaries. Achouri et al. (2013) explored the void nucleation in different stress states via visualizing the nucleation process and the micro-crack through in-situ tension and shear tests. Lin et al. (2018) discussed the effect of initial microstructure on nucleation and growth of voids of a nickel-based superalloy at intermediate temperatures via TEM examinations. Scott et al. (2017) conducted observations and quantitative analysis about the void evolution and declared that the primary coalescence model of closely spaced voids is internal necking while the coalescence of voids spaced farther apart is mainly from void sheeting. In the study of Taylor and Sherry (2012), the void volume fraction (VVF) was quantified and the failure was identified to occur when a critical VVF is reached. For the void behavior in pure magnesium, Nemcko et al. (2016) concluded that local microstructures, including grain boundaries and twins notably affect the growth and linkage of voids while the influence of initial void volume fraction is limited. Through experimental characterizations, Kondori et al. (2018b) demonstrated that the growth of void in magnesium alloy is anisotropic.

Apart from experimental observations, modeling of the behaviors of voids is also an essential way to understand the void behavior. For the growth of spherical voids, Rice and Tracey (1969) considered the contribution of both volume and shape changes and related void growth to remote strain and stress triaxiality. The Gurson–Tvergaard–Needleman (GTN) porous plasticity theory (Gurson, 1977; Tvergaard, 1981; Tvergaard and Needleman, 1984) developed on the basis of micromechanics theories has been widely used for characterizing

the yield surface and void behavior of porous materials. The GTN model has attracted a lot of interests since developed and some efforts were conducted to extend its application range (Nahshon and Hutchinson, 2008; Besson, 2009b). Alinaghian et al. (2014) took into account the effect of pre-strain and work hardening rate on void growth and established a model which is capable of capturing the correlation between void behavior and pre-strain. To model the void growth in polycrystalline materials, Lebensohn et al. (2013) put forward a computing method. Concerning the modeling of void coalescence, the Thomason model (Thomason, 1985a, b), and its extended form proposed by Pardoen and Hutchinson (2000) have been extensively utilized. Based on the analytical analysis, Torki (2019) developed a yield criterion to describe both the void growth and coalescence in the stress state of combined tension and shear. In recent works, the modeling of the evolution of ellipsoidal voids in viscous metals has also been conducted (Feng and Cui, 2015; Lin et al., 2016).

Validations of the void models were carried out by using both experiment and simulation approaches. Weck et al. (2008) provided an in-depth experimental validation for various void models by visualizing void growth and coalescence in sheets containing laser-drilled holes. Hosokawa et al. (2013) evaluated the performance of various void coalescence models and concluded that the existing void coalescence models assuming a periodic cubic array give an upper bound solution of the ductility materials with arbitrarily arranged voids. The results of simulations coupled with the GTN model conducted by Ueda et al. (2014) indicated that the GTN model overpredicts the void growth in deformation. Landron et al. (Landron et al., 2011; Landron et al., 2013) experimentally assessed the modified Rice and Tracey void, the Brown and Embury model, and the Thomason model, and validated that the Thomason coalescence model is more adapted for predicting the local coalescence events.

It is well known that the grain-scale heterogenous deformation resulted from microstructure has a non-negligible effect on the behavior of materials. Through novel test approaches, the heterogeneous strain field on the micro-scale was experimentally investigated for metal polycrystals (Sachtleber et al., 2002; Morgeneyer et al., 2014; Guery et al., 2016; Fujita et al., 2018). In the study of the grain-scale material's behavior, the CP based simulation technique is very helpful. CPFE simulation has been extensively used to articulate the micro-scale characteristics, for instance, to study the strain and stress heterogeneity (Abdolvand et al., 2015; Zhang et al., 2018; Tang et al., 2019), to identify texture evolution and anisotropy of materials (Raabe et al., 2007; Jia et al., 2012; Li et al., 2017; Kondori et al., 2018a), and to investigate the twinning induced plasticity (Sun et al., 2016). In terms of the microstructure affected void behavior, Kadkhodapour et al. (2011) figured out that the morphology and distribution of martensite particles dominate the void evolution and failure mechanism via adopting both the experiment and CPFE simulation methods. Selvarajou et al. (2019) applied the CPFE method in studying the implications of slip and twinning of hexagonal close packed crystals on void behavior. Regarding the influence of grain evolution on void behavior, Shang et al. (2017) demonstrated that the occurrence of dynamic recrystallization in hot deformation greatly affects the void behavior and improves the ductility of metals.

As a result, figuring out the effect of microstructure on void behavior is essential for an in-depth understanding of the relationship between microstructure and macroscopic fracture. This study thus aims at identifying the effect of grain structure on the micro-void behavior and macroscopic fracture via experiment and CPFE modeling. Experimentally, the grain structure and voids were examined by SEM and EBSD. In accordance with the experimental results, a three-dimensional CPFE model embedding voids was established. The influence of grain size on deformation heterogeneity, void growth, and void coalescence was identified

and quantitatively analyzed, and a formulation considering the effect of grain size was developed to predict the distribution of major void diameter. With the grain structure affected deformation and void evolution, the macroscopic fracture of materials was also shown to be grain size dependent. The relationship between grain size and ductility was carefully examined and discussed in this study.

2. Experiment and CPFE modeling

2.1 Experiment

The testing material selected for this research is the as-forged 316LN stainless steel which possesses a mono-austenite microstructure. Since the testing material does not show phase transformation and multi-phase induced heterogeneous deformation, its property is thus mainly affected by grain structure. The microstructure of material was first examined by SEM and EBSD, and the results are shown in Fig. 2. Fig. 2(a) presents the orientation imaging microscopy (OIM) images from EBSD results for the areas with the grain size of 42.6 and 116 μm. According to the OIM results, the grains of the as-forged 316LN steel have a uniform orientation distribution. Small voids and inclusions with a roughly spherical shape are observed inside the matrix, as shown in the SEM results in Fig. 2(b). The defects of voids and inclusions in the materials serve as the crack source in plastic deformation. To investigate the void evolution during plastic deformation, uniaxial tensile tests with different strain levels were conducted using cylindrical samples (Fig. 3) and the characterization of voids under different strain levels was done. In addition, the feature of fracture surface of the samples with different grain sizes was compared.

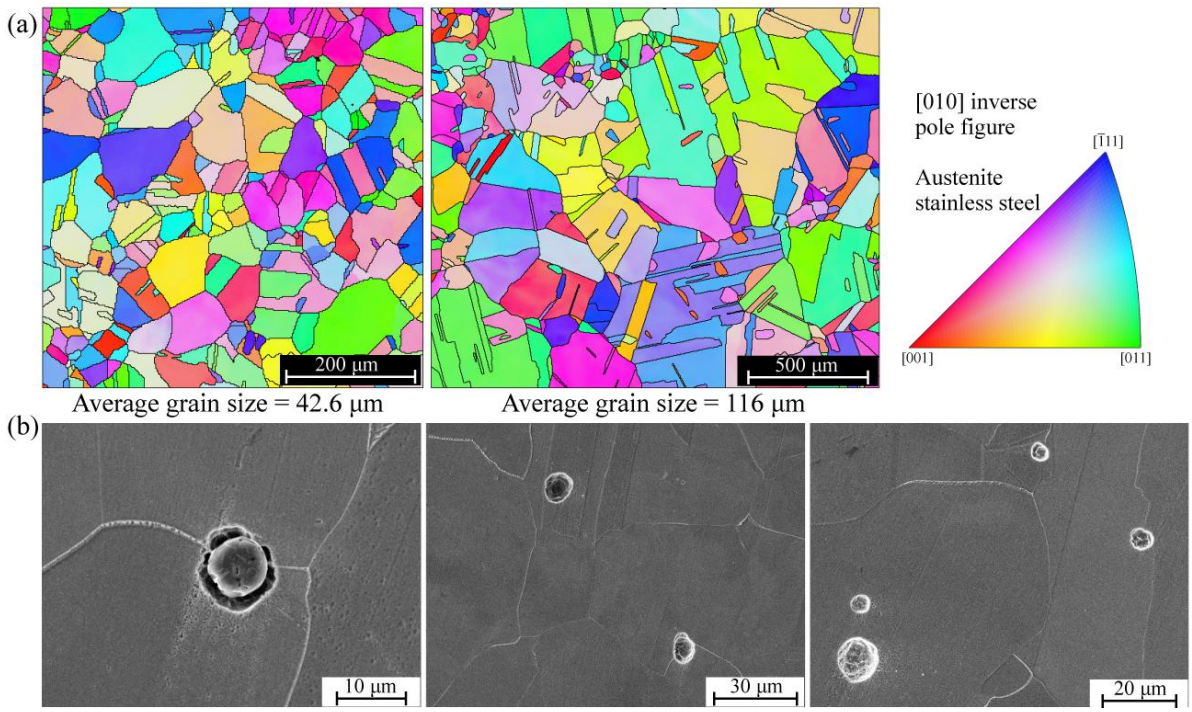

Fig. 2. Microstructure of as-forged 316LN stainless steel used in this research: (a) OIM images from EBSD showing different grain sizes and orientations, and (b) the voids and inclusions observed by SEM inside the material.

2.2 Crystal plasticity based constitutive model

The constitutive equation in crystal plasticity (CP) describes the relationship between shear rate and shear stress in plastic deformation. This research adopts a phenomenological rate-dependent flow law in a finite strain CP framework (Zhang et al., 2012; Zhang et al., 2018) to describe the slip rate of the α -th slip system:

$$\dot{\gamma}^{\alpha}=\dot{\gamma}_0\left(\frac{\left|\tau^{\alpha}\right|}{g^{\alpha}}\right)^{1/m} sgn\left(\tau^{\alpha}\right) \tag{1}$$

where $\dot{\gamma}_0$ is the reference slip rate and τ^{α} the resolved shear stress acting on the slip system. m represents the strain rate sensitivity and g^{α} is the slip resistance which increases asymptotically from the initial value g_0 towards the saturation value g_s . To

represent the work hardening behavior of crystal materials, a reasonable expression of g^{α} is important. The evolution of g^{α} is formulated by the rate form hardening in the following:

$$\dot{g}^{\alpha} = \sum_{\beta=1}^{n} h_{\alpha\beta} \left| \dot{\gamma}^{\beta} \right| \tag{2}$$

where the strain hardening matrix $h_{\alpha\beta}$ can be expressed by a saturation law as:

$$h_{\alpha\beta} = h_0 \left[q + (1-q)\delta^{\alpha\beta} \right] \left| 1 - \frac{g^{\beta}}{g_s} \right|^{a_h} sgn\left(1 - \frac{g^{\beta}}{g_s} \right) \tag{3}$$

where $h_{\alpha\beta}$ is the self-hardening coefficient, $\delta^{\alpha\beta}$ the Kronecker delta and a_h the hardening exponent. q represents the interactive strength ratio between slip systems, which is set to 1.0 for coplanar slip systems and 1.4 for non-coplanar slip systems.

The resolved shear stress is related to the external stress imposed on the material point and designated as:

$$\tau^{\alpha} = \left(\mathbf{F}^{\mathbf{eT}} \mathbf{F}^{\mathbf{e}} \cdot \mathbf{T}^{\mathbf{e}} \right) : \mathbf{S}_0^{\alpha}, \text{ with } \mathbf{S}_0^{\alpha} = \mathbf{m}_0^{\alpha} \otimes \mathbf{n}_0^{\alpha} \tag{4}$$

where $\mathbf{F}^{\mathrm{e}}$ is the elastic part of the deformation gradient $\mathbf{F}$ which accounts for the elastic distortion of the crystalline lattice and the rotation of lattice. $\mathbf{T}^{\mathrm{e}}$ is the 2nd Piola-Kirchhoff stress tensor and $\mathbf{S}_0^{\alpha}$ is the Schmid tensor. $\mathbf{S}_0^{\alpha}$ is the Kronecker product of the unit vectors for slip direction ($\mathbf{m}_0^{\alpha}$) and the normal direction ($\mathbf{n}_0^{\alpha}$) of the slip plane. $\mathbf{T}^{\mathrm{e}}$ is in relation to the elastic Green strain tensor $\mathbf{E}^{\mathbf{e}}$ via the fourth order anisotropic elastic tensor $\mathbb{C}$:

$$\mathbf{T}^{\mathbf{e}} = \mathbb{C} : \mathbf{E}^{\mathbf{e}}, \text{ with } \mathbf{E}^{\mathbf{e}} = \left(\mathbf{F}^{\mathbf{eT}} \mathbf{F}^{\mathbf{e}} - \mathbf{I} \right) / 2 \tag{5}$$

where $\mathbb{C}$ is determined by the elastic parameters C_{11}, C_{12} and C_{44} of cubic crystals.

The CP model was coded into the FE software ABAQUS via the subroutine UMAT. Material

constants in the CP based constitutive model was calibrated by fitting the constitutive curve to the uniaxial tensile results. The determined parameters for the studied 316LN steel are listed in Table 1.

Table 1

Material constants in the CP model determined for the testing 316LN steel.

C_{11}	C_{12}	C_{44}	g_0	g_s	h_0	$\dot{\gamma}_0$	m	a_h
262.5 GPa	112.5 GPa	75.0 GPa	127.9 MPa	863.0 MPa	295.9 MPa	0.001 s^{-1}	0.02	2.113

2.3 Crystal plasticity modeling methodology

For a comprehensive understanding of the void behavior affected by grain structure, the tensile process of a three-dimensional representative volume element (RVE) with voids was simulated by the CP modeling. The RVE is a representative of the cylindrical sample, which was established by revolving part of the meridian plane around the symmetry axis with a small angle, as shown in Fig. 3. Spherical voids were embedded in the RVE, and the initial void volume fraction is assumed to be 0.658%. Although the existence of voids brings about non-axisymmetry to the RVE model, the model is still assumed to be axisymmetrical as the void volume is much smaller than the model volume. A uniaxial tensile boundary condition was applied on the RVE. In order to meet the constant volume principle, a radius displacement u_r was imposed on the inner surface vertical to the radius direction:

$$u_r = r_0 - \sqrt{\frac{\pi r_0^2 l_0}{\pi\left(l_0 + u_z\right)}} \tag{6}$$

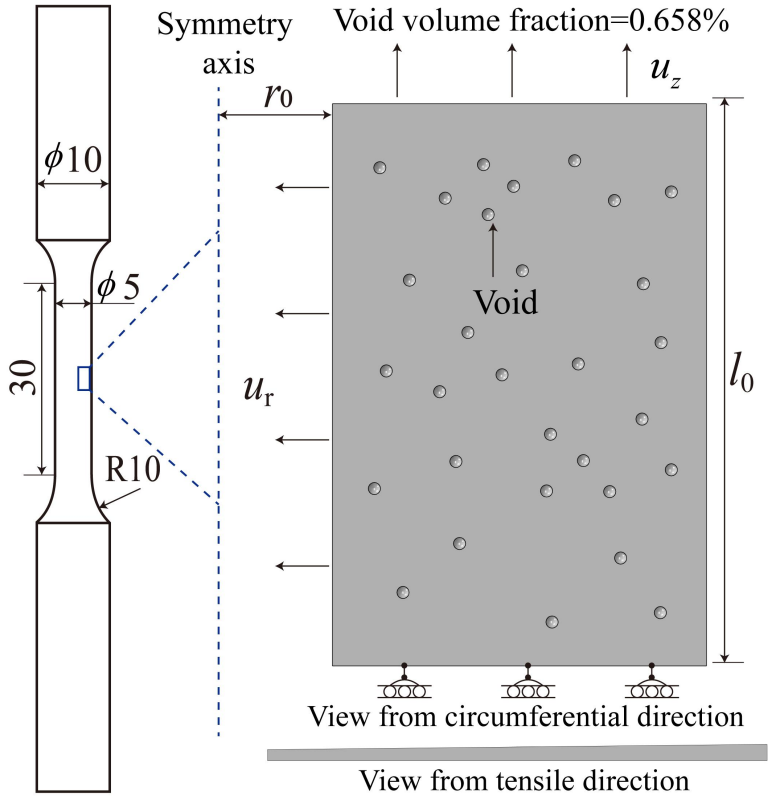

Fig. 3. Three-dimensional RVE containing voids subjected to a uniaxial tension test.

The RVE was carefully meshed by hexahedral elements and the element type C3D8R in ABAQUS was used for FE calculation. To identify the effect of grain size on void behavior and ductility, the deformation of the RVE with different grain sizes was simulated. Fig. 4 exhibits the mesh and the grains in the RVE with the grain size of 54, 110, 243 and 543 μm. A random orientation was assigned to grains. To avoid the contingency of the orientation assignment, thirty groups of orientations were set and tested for each grain condition. Upon the completion of simulation, the results of strain, stress and the void dimension data were examined to explore the grain size affected void behavior.

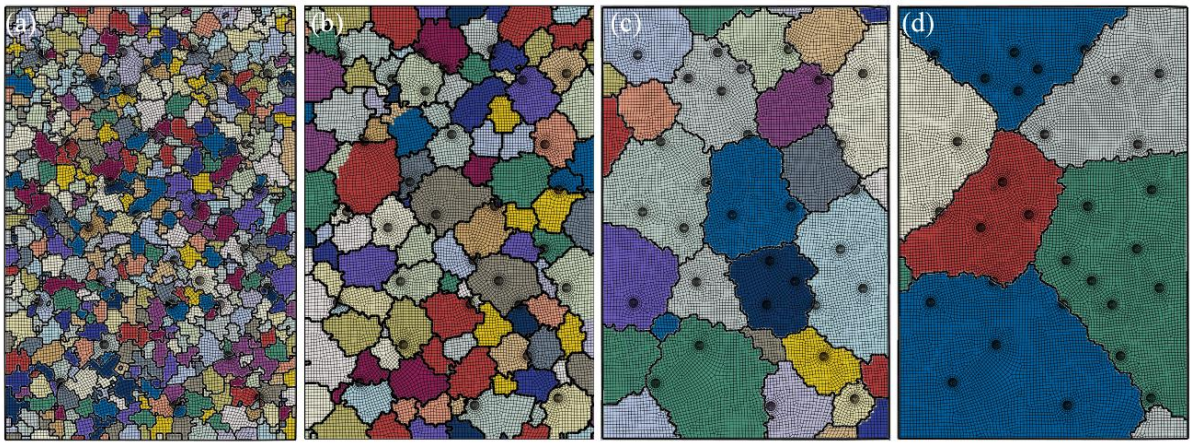

Fig. 4. RVE with different average grain sizes $\bar{d}$ (μm): (a) $\bar{d}$ =54, (b) $\bar{d}$ =110, (c) $\bar{d}$ =243, and (d) $\bar{d}$ =543.

The orientation distribution and evaluation of grain deformability of the RVEs with the grain size of 110 μm are shown in Fig. 5 as an instance of the grain structure modeling. The results of OIM image shown in Fig. 5(a) and the (111) pole figure in Fig. 5(b) indicate that pre-deformed RVEs have a weak texture. The deformability of individual grains in plastic deformation is related to their orientation with respect to the loading direction and the instantaneous Taylor factor is usually adopted to measure the deformability (Zhang et al., 2018). The Taylor factor is calculated by $M = \sum_{\alpha} \dot{\gamma}^{\alpha} / \bar{\mathbf{D}}^{\mathrm{p}}$ where $\bar{\mathbf{D}}^{\mathrm{p}}$ is the von Mises plastic deformation rate. The distribution of Taylor factor for the RVE subjected to the uniaxial tension is shown in Fig. 5(c). Area with the larger M is harder to be deformed.

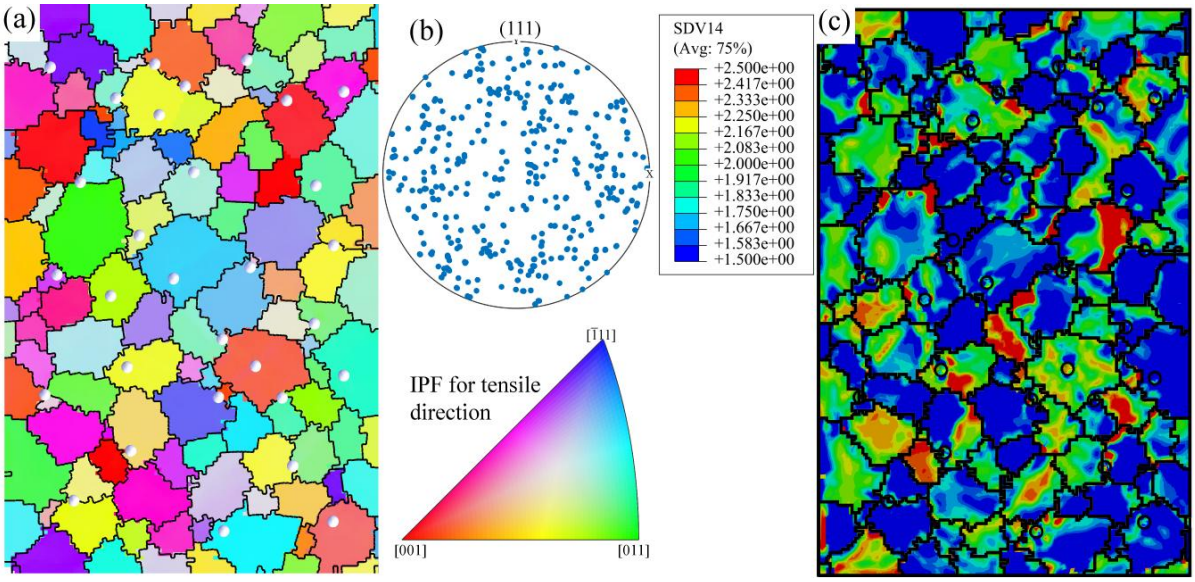

Fig. 5. Grain structure modeling for the RVE with the grain size of 110 μm: (a) OIM of the RVE, (b) (111) pole figure, and (c) distribution of Taylor factor in uniaxial tensile loading.

3. Results and discussions

3.1 Experimental results

The experimental results were first examined to identify the deformation heterogeneity and the characteristic of uniaxial fracture surface of the studied material with different grain sizes. Fig. 6 presents the surface morphology of cylindrical samples with different sizes of grains after uniaxial tension. Roughening is clearly observed on the outer surface which is a proof of the microscopic deformation heterogeneity. The surface roughness of the coarse grain sample is more evident than that of the fine grain sample, indicating that the deformation is more heterogeneous for coarse grain materials.

Morphology of the uniaxial fracture surface for the samples with different grain sizes is exhibited in Fig. 7. An obvious difference of the topography of fracture surface is shown for the samples with the grain size of 28 and 190 μm. The fracture surface of the sample with the grain size of 28 μm has a typical cup-cone morphology with the dimple region, the shear

region, and the transition region. Dimples correspond to the material's internal voids. At the dimple region, a large number of relatively deep dimples are observed, while in the shear region, the dimples are shallow, which indicates a limited void growth. As for the sample with the larger grain size of 190 μm, the fracture surface is no longer of a cup-cone morphology. There are very large and deep dimples, which correspond to very large voids, appearing at the center as well as the edge area of sample. A detailed explanation for the variation of fracture surface topography with grain size is provided in section 3.5 according to the results of CP modeling.

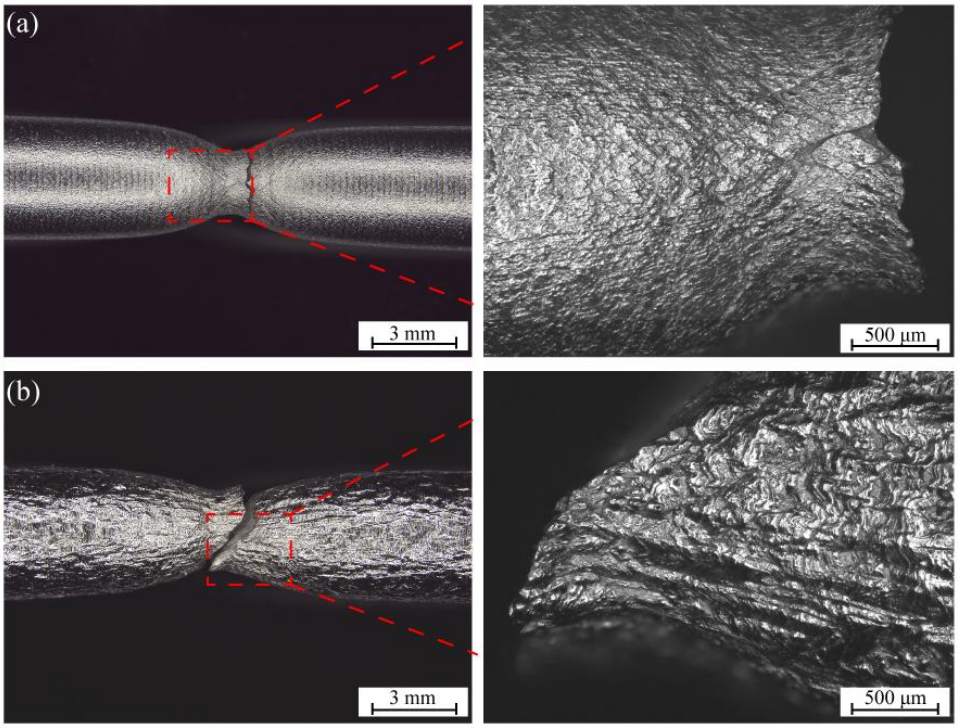

Fig. 6. Surface topography of cylindrical samples after uniaxial tensile test: (a) the sample with the grain size of 28 μm, and (b) the sample with the grain size of 190 μm.

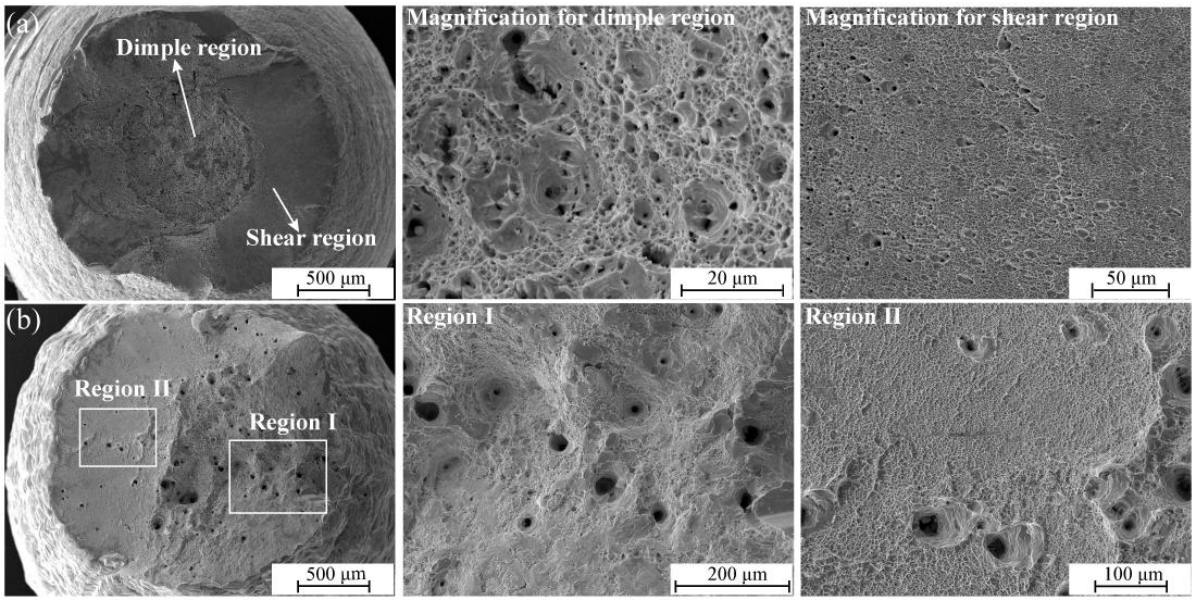

Fig. 7 Morphology of the uniaxial tension fracture surface for samples with different grain sizes: (a) the sample with the grain size of 28 μm, and (b) the sample with the grain size of 190 μm.

To characterize the void growth in plastic deformation, tensile experiments with different strains ε were conducted and the voids in longitudinal section of the cylindrical samples were examined by SEM and exhibited in Fig. 8. The results indicate an evident growth of void in plastic deformation. In the beginning of deformation, voids and inclusions have a roughly spherical morphology with the diameter of about 10~20 μm, as shown in Fig. 2. At the small tensile strain (ε =0.148 and 0.278 for instance), voids grow slightly and show a roughly ellipsoid shape. Some inclusions still remain in the matrix. At the larger global strains (ε =0.392 and at the final fracture), however, voids grow significantly and show an obvious elongation along the tensile direction. In addition, the cracks of the matrix materials can be clearly observed inside some voids. Furthermore, a severely elongated void with the major diameter larger than 80 μm in the longitudinal section of the fracture sample is observed.

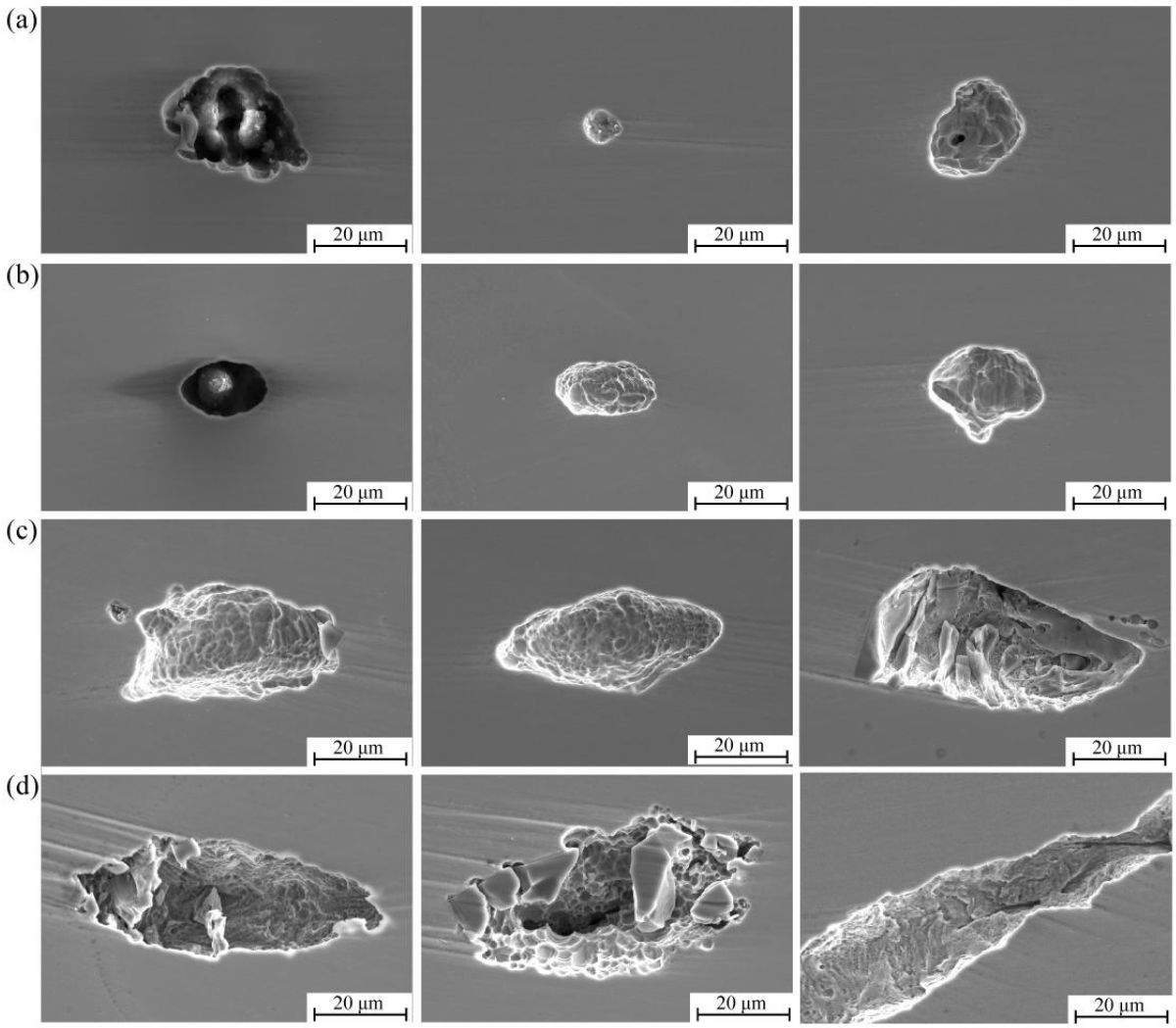

Fig. 8. SEM results of the voids in the longitudinal section of the cylindrical sample with the grain size of 190 μm at different global strains ε: (a) ε=0.148, (b) ε=0.278, (c) ε=0.392, and (d) ductile fracture. The magnification is 5000.

3.2 Deformation characteristics in tensile deformation

During the plastic deformation of metallic polycrystals, grains rotate primarily to accommodate the deformation and constraint imposed by the macroscopic boundary conditions as well as the microscopic interaction between grains. The deformation characteristics and grain rotation during the tensile process are first examined, and the result of the RVE with grain size of 110 μm is taken as a representative and shown in Figs. 9 and 10.

According to the OIM images and inverse pole figures of the RVE at different strain levels, a typical texture evolution of uniaxial tension is shown for the RVE, *i.e.*, with the proceeding of tension deformation, most grains rotate to make the tensile axis parallel to the crystal axes of [111] or [100]. Voids grow during the plastic deformation and become elongated along the tensile direction.

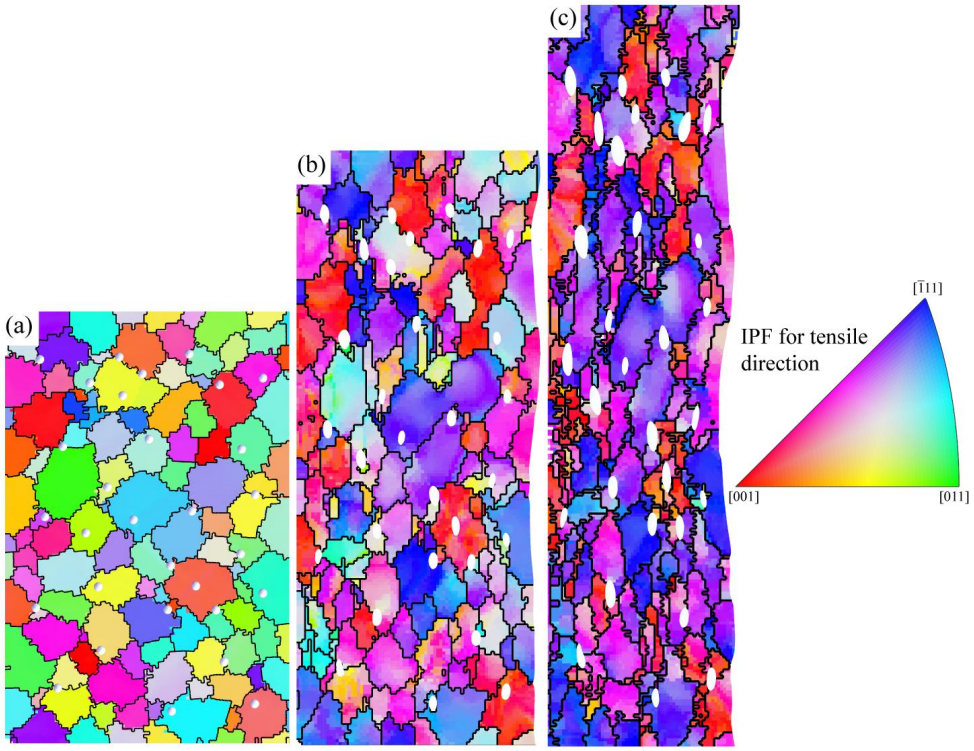

Fig. 9. OIM for the RVE with the grain size of 110 μm at different global strains ε: (a) ε=0, (b) ε=0.3465, and (c) ε=0.693.

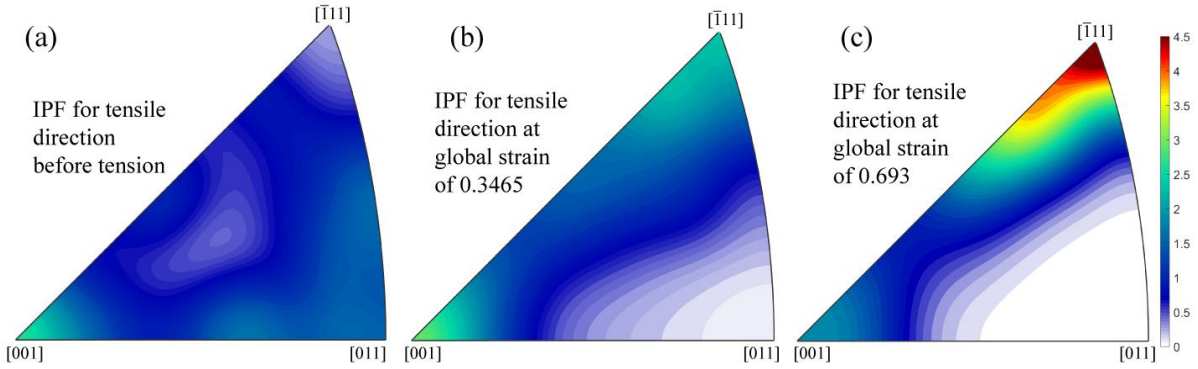

Fig. 10. Inverse pole figure for the RVE with the grain size of 110 μm at different global strains ε: (a) ε=0, (b) ε=0.3465, and (c) ε=0.693.

3.3 Influence of grain size on deformation and void growth

To explore the effect of grain structure on deformation and void behavior, the tensile process of RVEs with different grain structures is simulated. In the research, the grain structure stands for the grain size and grain orientation. For comparison, the deformation of uniform RVE with a constant stress-strain relation was simulated by general FE simulation in which the grain structure was not involved. The distribution of equivalent plastic strain of the uniform RVE exhibited in Fig. 11(a) indicates that the deformation of uniform RVE is relatively homogeneous with the concentration of deformation only appearing inside the voids. While for the RVEs involving grain structure shown in Figs. 11(b)-(e), microscopic deformation heterogeneity occurs due to the variation of deformability of grains with different crystal orientations. During plastic deformation, the grain structure involved RVE can be divided into 'soft' and 'hard' areas in accordance with the grain orientation with respect to the loading direction. Deformation is more likely to concentrate in 'soft' areas. In the RVE with the smaller grain size of 54 μm, there are a number of narrow deformation bands about 45° relative to the tensile direction. As the grain size is increased, the deformation bands become wider but the number of which is decreased, resulting in the deformation concentration at the larger continuous regions. Therefore, as the grain size is increased, the deformation heterogeneity becomes more obvious. Sags and crests appear at the free edge of RVEs involving grain structure, which correspond to the roughness of the sample surface observed in experiments shown in Fig. 6.

Void behavior is closely related to deformation heterogeneity. In the uniform RVEs, the morphology and size of voids in different regions are almost the same. This phenomenon conflicts with the experimental observations of the different sizes and morphologies of voids at a certain deformation stage shown in Fig. 8. Therefore, without the consideration of grain

structure and crystal orientation, the variation of void growth cannot be captured correctly. For the RVEs involving grain structure, voids in the main deformation zone undergo a large growth while the voids in the small deformation areas grow slightly. As the deformation heterogeneity is increased with grain size, the variation of void size also becomes more obvious at the large grain condition. Similarity is shown for the deformation pattern in terms of the roughness in free surface of samples in experiments (Fig. 6) and the CP simulation results involving grain structure. In addition, the void morphology in the CP modeling with the consideration of grain structure is similar to the experimental ones exhibited in Fig. 7.

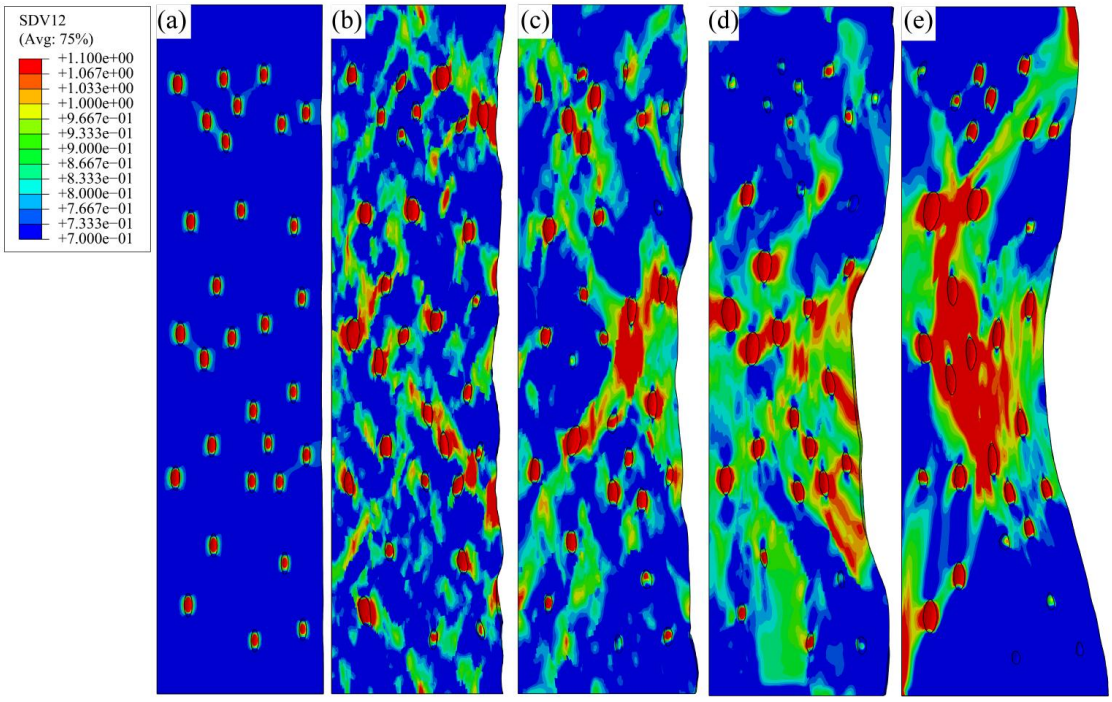

Fig. 11. Distribution of equivalent plastic strain for RVE with different grain sizes $\bar{d}$ (μm) at the global strain of 0.693: (a) uniform matrix without grain structure, (b) $\bar{d}$ =54, (c) $\bar{d}$ =110, (d) $\bar{d}$ =243, and (e) $\bar{d}$ =543.

The distribution of von Mises stress in the RVEs with different grain sizes is shown in Fig. 12. For the RVEs considering grain structures, the distribution of Mises stress is different from the strain distribution shown in Fig. 11, as the large deformation zone is usually the ‘soft’ area

and the work hardening is not the only influential factor for the induced stress. No obvious correlation between void growth and the stress distribution is observed. For instance, the voids in the stress concentration zone marked in Figs. 12(d) and (e) are smaller than that in the area with less stress concentration marked in Fig. 12(d). The close relation between void evolution and deformation and the obscure correlation between void evolution and stress are the truth for all the studied cases. Therefore, the void behavior of materials might be more related to local strain concentration than to stress concentration.

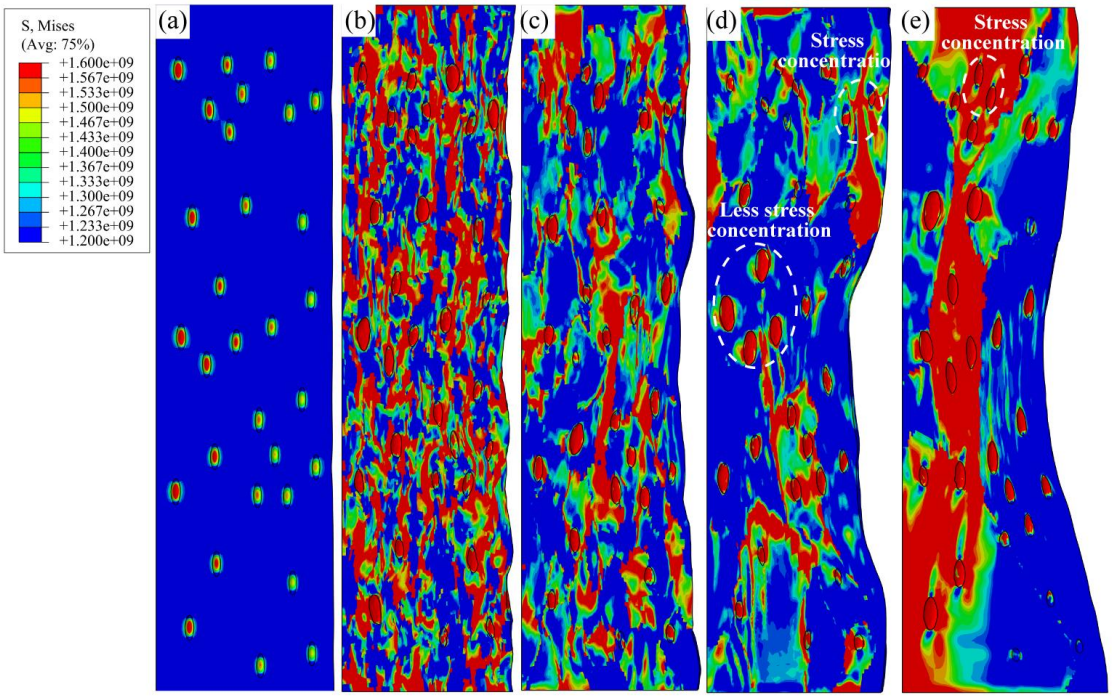

Fig. 12. Distribution of von Mises stress for RVE with different grain sizes $\bar{d}$ (μm) at the global strain of 0.693: (a) uniform matrix without grain structure, (b) $\bar{d}$ =54, (c) $\bar{d}$ =110, (d) $\bar{d}$ =243, and (e) $\bar{d}$ =543.

To get an insight into the effect of grain size on void growth, the quantitative data about voids in different grain size conditions was analyzed and compared. The RVEs with the grain size of 54 and 543 μm were selected as representatives for fine grain (FG) and coarse grain (CG) scenarios and the evolution of the normalized void volume (V / V_0) and the normalized major

void dimension (a / a_0) for large and small voids in CG and FG conditions is presented in Fig. 13. The frequency distribution and the average value of V / V_0 , a / a_0 for all the voids in CPFE simulations for CG and FG RVEs at the global strain of 0.693 are shown in Fig. 14. According to the modeling results, voids in the RVEs grow gradually during plastic deformation. In the CG RVE the voids show more evident differences in terms of both the growth rate and the resulting void size. The larger the grain size, the larger possibility of the occurrence of non-uniform void size. In general, large voids have a more pronounced effect on formation of macroscopic ductile fracture. Compared with V / V_0 , a / a_0 is more measurable and the established void growth models generally described the evolution of a / a_0 in plastic deformation.

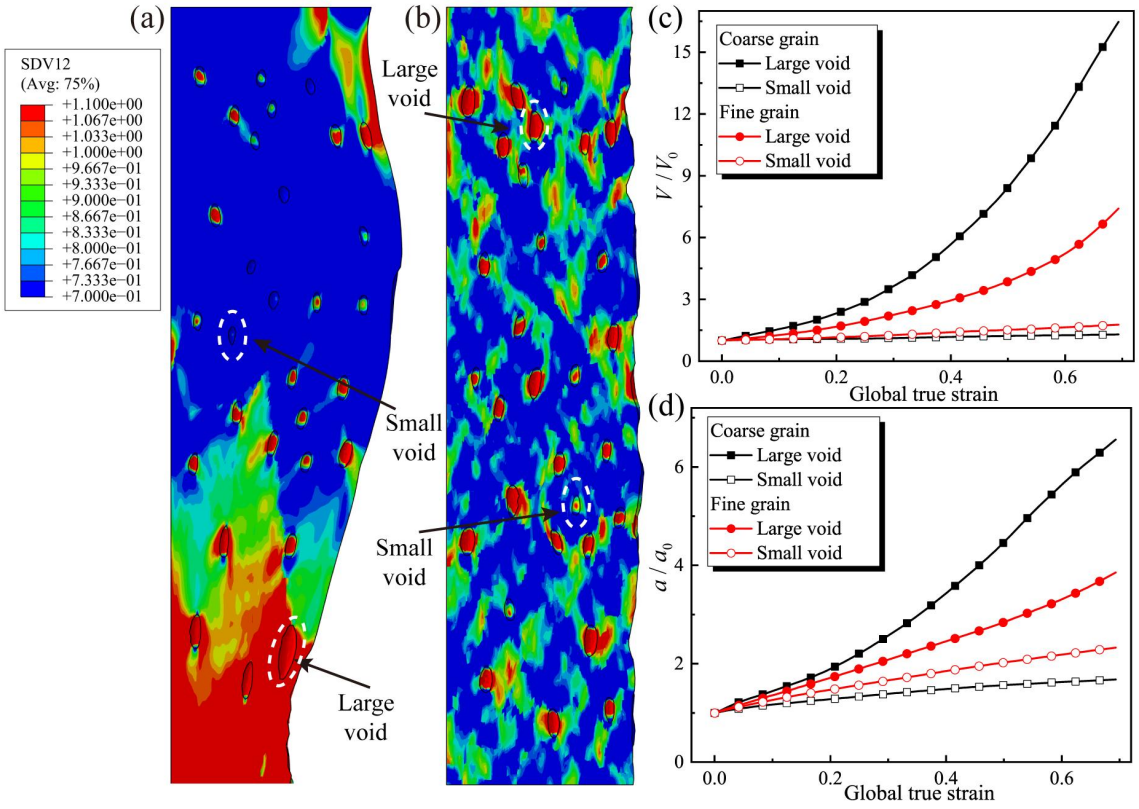

Fig. 13. Variation of void dimensions in the CG and FG RVEs: (a) the equivalent plastic strain in the CG RVE, (b) distribution of the equivalent plastic strain in the FG RVE, (c) evolution of normalized void volume for large and small voids, and (d) evolution of normalized major void diameter for large and small voids.

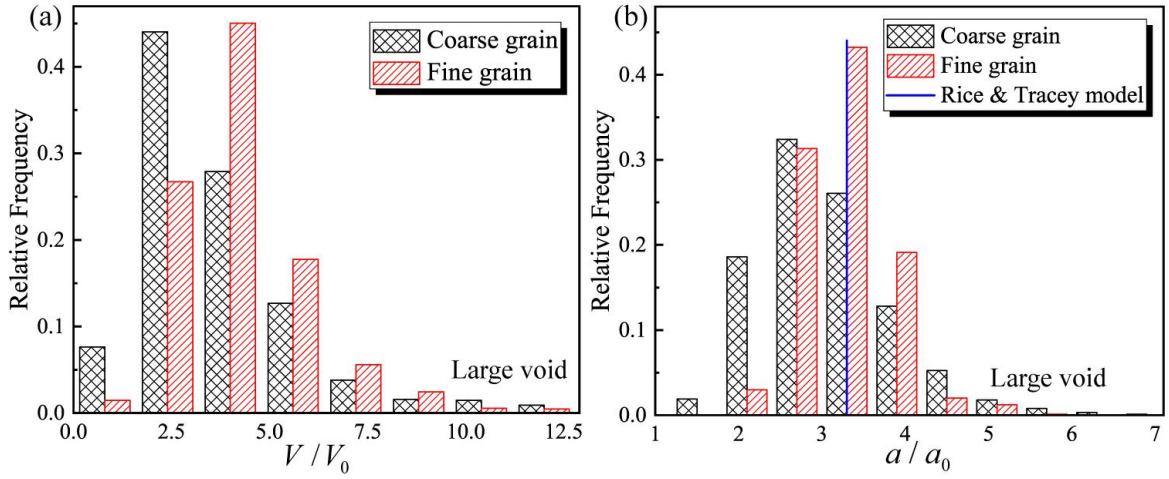

Fig. 14. Frequency distribution of (a) normalized void volume, and (b) normalized major void dimension for the CG and FG RVEs at the global strain of 0.693.

The non-uniform void size is closely related to the heterogeneity of the plastic deformation. The frequency distribution of the equivalent plastic strain shown in Fig. 15(a) indicates that plastic deformation is more non-uniform in the CG condition. For the CG RVE, as shown in Fig. 13(a), strain localizations obviously take place in the regions with identical orientations which results in the evident necking zone. Grains outside the necking zone experience a relatively small deformation and the growth of voids in these regions is thus limited. With the more non-uniform deformation in the CG scenario, the distribution of stress is also more heterogeneous and the region possessing smaller and larger stress is larger, as presented in Fig. 15(b).

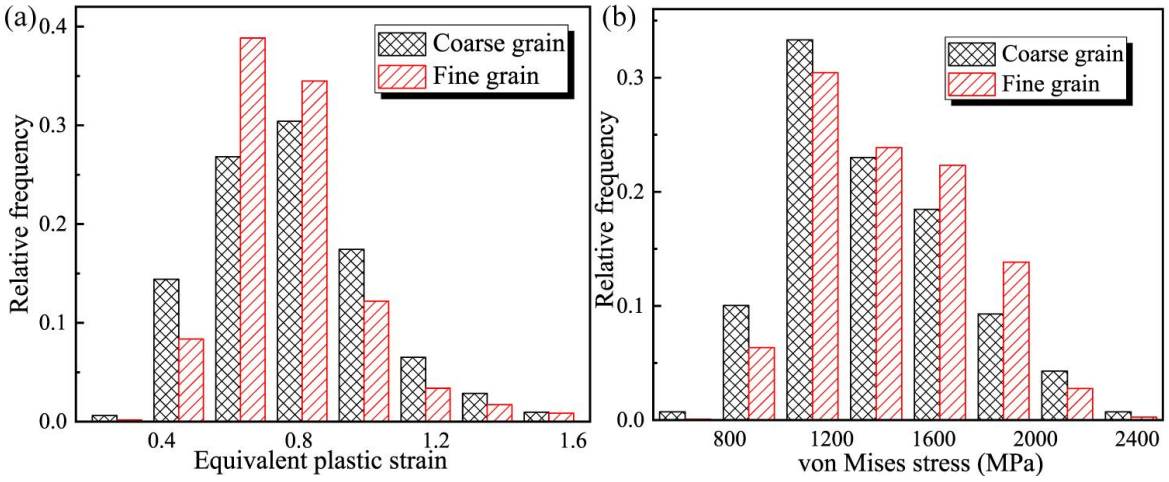

Fig. 15. Frequency distribution of (a) equivalent plastic strain, and (b) von Mises stress for the CG and FG RVEs at the global strain of 0.693.

3.4 Extended void growth model considering the effect of grain size

To characterize the non-uniform void size and the effect of grain size on void growth, the classical Rice and Tracey model describing the growth of void in plastic deformation is modified in this study. The Rice and Tracey model relates the void growth to the remote strain and stress triaxiality, and the integrated form of the model is designated in the following:

$$\frac{a}{a_0} = \exp\left(D\varepsilon_1\right) + \left(\frac{1+E}{D}\right)\left(\exp\left(D\varepsilon_1\right) - 1\right) \tag{7}$$

$$\frac{b}{b_0} = \exp\left(D\varepsilon_1\right) - \frac{1}{2}\left(\frac{1+E}{D}\right)\left(\exp\left(D\varepsilon_1\right) - 1\right) \tag{8}$$

where a and b are the major and minor void diameters respectively, ε_1 is the remote logarithm plastic strain. D and E characterize the volume and shape changing of the void. D is formulated as:

$$D = 0.558\sinh\left(\frac{3}{2}\eta\right) + 0.008\cosh\left(\frac{3}{2}\eta\right) \tag{9}$$

where η is the stress triaxiality which is represented as σ_m / σ_y. σ_m is the mean stress

and σ_y is the yield stress. According to relation between D and E provided by Rice and Tracey (1969), E is set to 2 in this work.

Fig. 16 shows the evolution of η, and the comparison of a/a_0 based on the Rice and Tracey model and the CPFE modeling results for the voids in RVEs as shown in Fig. 13. According to the simulated and predicted results of a/a_0 shown in Figs 14 and 16, the prediction of a/a_0 by the Rice and Tracey model at a certain global strain is a constant value while the simulated ones fluctuate. To extend the Rice and Tracey model for describing the non-uniform void growth, the regularity of void size distribution was carefully examined and the results for RVE with grain size of 110 μm at different strain levels are shown in Fig. 17. The results of a/a_0 distribution in RVEs with the grain size of 54, 110 and 543 μm shown in Figs 14(b) and 17 demonstrate that a Gaussian function is able to describe the distribution of a/a_0 at a wide range of grain size and global strain scenarios. Moreover, both the average value and the standard error of a/a_0 are increased with the global strain.

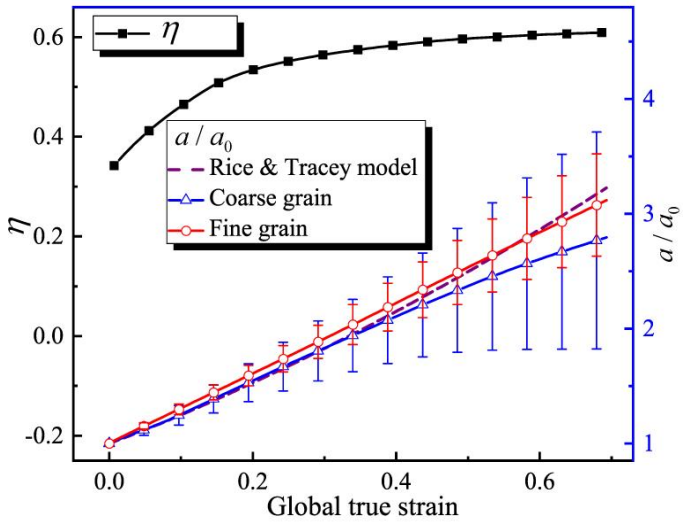

Fig. 16. Evolution of η, simulated a/a_0 as well as predicted a/a_0 by the Rice and Tracey model in CG and FG RVEs.

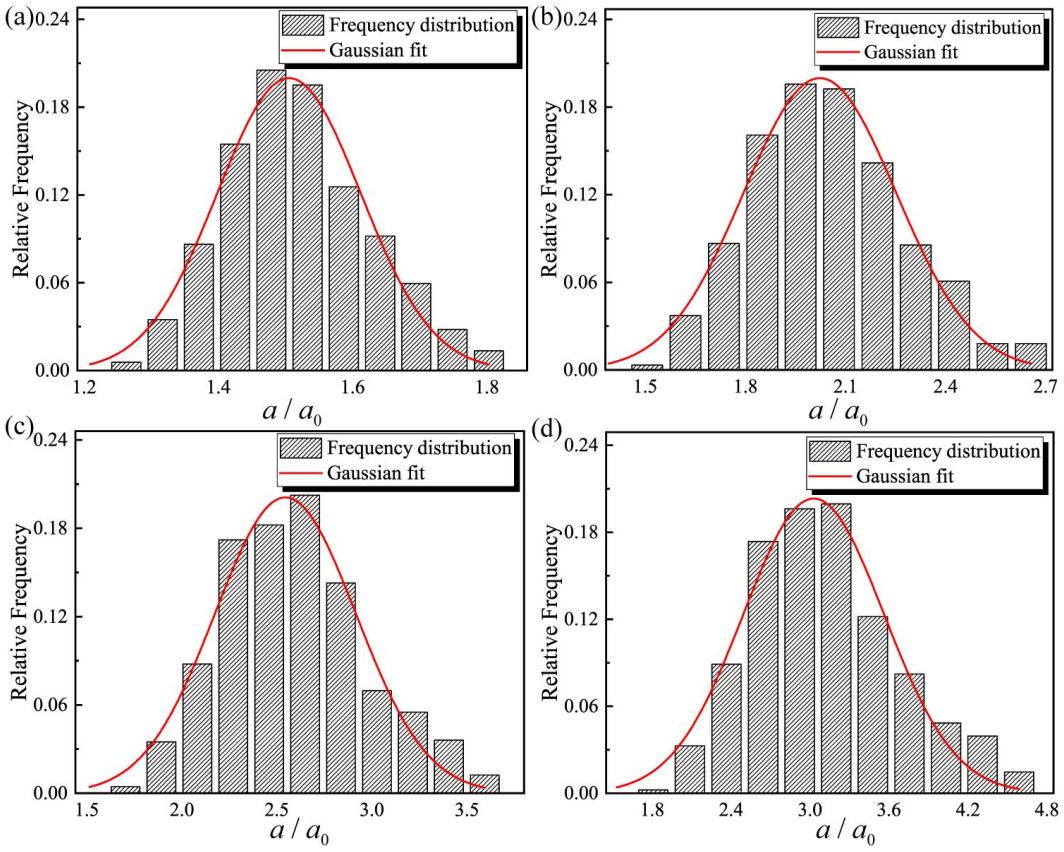

Fig. 17. Frequency distribution and the Gaussian fit of a / a_0 in RVE with grain size of 110 μm at different global strains: (a) ε=0.173, (b) ε=0.3465, (c) ε=0.519, and (d) ε=0.693.

Consequently, the distribution of a / a_0 in the RVEs with various grain sizes (54, 110, 243 and 543 μm) at different strain levels (0.173, 0.3465, 0.519, 0.693) was fitted by the Gaussian function. The expectation and the standard error of a / a_0 in different grain sizes and global strain scenarios were identified, as shown in Figs. 18(a) and (b). The expectation of a / a_0 is increased with the strain and decreased with the increase of grain size. Regarding the standard error of a / a_0, it is increased with both the strain level and grain size. The change of expectation and standard error of a / a_0 with the logarithm of grain size is well fitted by linear functions, and the linear curves at different strains are almost parallel. Therefore, the distribution of a / a_0 in RVEs with the average grain size of $\bar{d}$ subjected to the global

strain of $\bar{\varepsilon}_p$ can be described as:

$$f\left(a/a_0\right)=\frac{A}{\sigma_{a/a_0}\sqrt{2\pi}}\exp\left(-\frac{\left(a/a_0-\mu_{a/a_0}\right)^2}{2\left(\sigma_{a/a_0}\right)^2}\right) \tag{10}$$

$$\mu_{a/a_0}=A_1\cdot\ln\left(\bar{d}\right)+A_2 \tag{11}$$

$$\sigma_{a/a_0}=B_1\cdot\ln\left(\bar{d}\right)+B_2 \tag{12}$$

where $f\left(a/a_0\right)$ is the probability density function, μ_{a/a_0} and σ_{a/a_0} are the expectation and standard error of a/a_0. A_1, B_1 were calculated based on the average slope of expectation and standard error of a/a_0 at different strains shown in Fig. 18 and the calculation result is $A_1=-0.07736$, $B_1=0.04868$.

By means of combining the Gaussian function and the Rice and Tracey void growth model, an extended model was proposed to predict the distribution of a/a_0 in the materials with different grain sizes. To determine A_2, B_2 in the model, a critical grain size condition for uniform deformation is needed. As the deformation heterogeneity becomes less obvious with the decrease of grain size, the void behavior in the RVEs with infinitesimal grains will be similar as the ones in the uniform matrix shown in Fig. 11(a). In the uniform matrix, the growth of voids can be predicted by the original Rice and Tracey model with the standard error of a/a_0 approaching zero. The smallest grain size considered in this research is 54 μm. In this grain size condition, the non-uniform deformation and void size still exist. For the convenience of parameter calibration, $\bar{d}=1$ is assumed as the critical condition for uniform deformation. By adopting this assumption, the parameter A_2 in Eq. (11) corresponds to the predicted result of the Rice and Tracey model and the standard error of void dimension, *i.e.*, the parameter B_2 in Eq. (12) is zero. With the CPFE simulated results and the assumption

of $\bar{d}=1$ as the critical condition of uniform deformation, the average value and standard error of a/a_0 for the testing material are described as:

$$\mu_{a/a_0} = -0.07736 \cdot \ln\left(\bar{d}\right) + \left(a/a_0\right)_{Rice\&Tracey} \tag{13}$$

$$\sigma_{a/a_0} = 0.04868 \cdot \ln\left(\bar{d}\right) \tag{14}$$

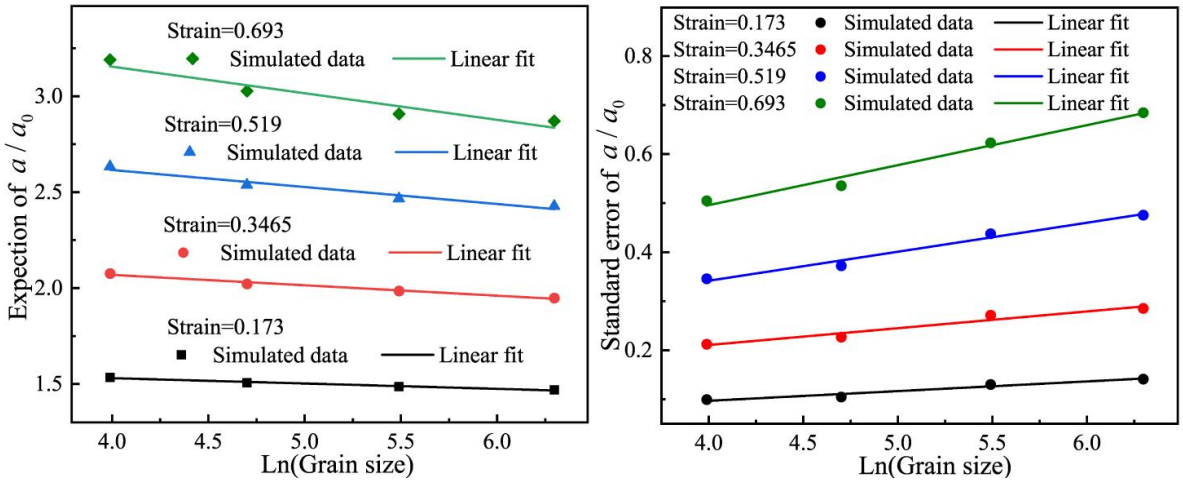

Fig. 18. The expectation and standard error of the Gaussian fit for simulated a/a_0 in RVEs with different grain sizes at different strain levels and corresponding linear fit.

3.5 Influence of grain size on void coalescence and morphology of fracture surface

The macroscopic ductile fracture of metals generally involves the microscopic coalescence of voids at large deformation. During plastic deformation, voids grow gradually and the speed of void growth is closely related to the strain localization in polycrystal metals. When a critical condition is met, the coalescence of voids takes place, which further prompts the formation of ductile fracture. Figs. 19(a) and (b) exhibit the fracture surface formed by the coalescence of voids in two RVEs with different grain sizes. The simulated fracture surface shows a zig-zag morphology, which coincides with the experimental result shown in Fig. 19(c). The formation of the zig-zag fracture surface is concluded to be caused by the random distribution of voids as well as the plastic heterogeneity. Additionally, we adopt the classical Thomason coalescence model (Thomason, 1985a, b) to evaluate the condition of void

coalescence. The Thomason model describes the plastic limit-load failure of inter-void matrix and considers the void coalescence taking place when the limit-load reaches a critical constraint factor. The Thomason model for uniaxial tension contains the part representing the effect of void dimension and the remote strain f_{T1}, and the part relating to stress state f_{T2}:

$$f_{T1}\left(a,b,e,\varepsilon_1\right)=\left(\frac{0.1}{\left(a/e\right)^2}+\frac{1.2}{\left(b/\left(b+e\right)\right)^{1/2}}\right)\frac{1}{\left(1-V_f\right)}\left(1-\left(\frac{3\sqrt{\pi}V_f}{4}\right)^{2/3}\left(\frac{b}{b_0}\right)^2\right)\exp\left(\varepsilon_1\right) \quad (15a)$$

$$f_{T2}\left(\sigma_{ij}\right)=\eta+\frac{2}{3} \quad (15b)$$

where $2e$ is the inter-void distance, V_f the initial void volume fraction, and ε_1 the tensile plastic strain. The coalescence of void is considered to occur when $f_{T1}=f_{T2}$.

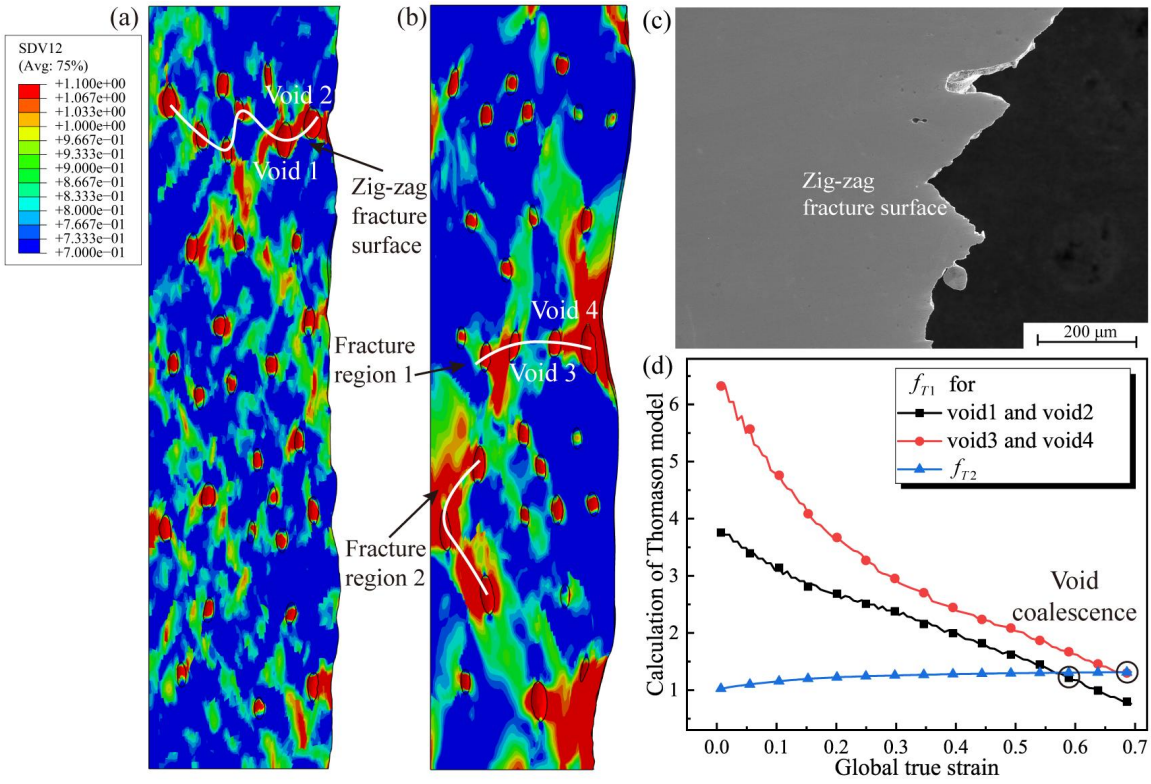

Fig. 19. Fracture induced by void coalescence: (a) distribution of the equivalent plastic strain in the RVEs with the grain size of 54 μm, (b) distribution of the equivalent plastic strain in the RVEs with the grain size of 243 μm, (c) experimental zig-zag fracture surface, and (d) the void coalescence predicted by the Thomason model.

The coalescence of 'void1' and 'void2' in Fig. 19(a) and 'void3' and 'void4' in Fig. 19(b) was taken as representatives and evaluated based on the Thomason model. f_{T1}, f_{T2} in deformation were calculated and the point of equality is the coalescence point, as shown in Fig. 19(d). According to the results, void coalescence does take place between the analyzed voids and the coalescence of a series of micro-voids eventually results in the macroscopic fracture. For the fracture formation area in the RVE shown in Fig. 19(b), there are two possible areas. In fracture region 1, coalescence occurs between voids possessing the relative similar dimensions. While in fracture region 2, the very large voids play an important role on fracture formation. The coalescence of very large voids is more commonly seen in the CG RVEs as the deformation in this scenario is more uniform. For the general materials, there are also many randomly distributed tiny voids which are arranged in ligament between the very large voids to serve as the bridge for the linkage of these large voids, as shown schematically in Fig. 20(a). Therefore, coalescence can take place between large voids with a large distance. As for the fine grain condition, the deformation is relatively uniform and the variation of void size is smaller than that in the CG RVEs. Fig. 20(b) presents the coalescence of voids with the smaller size variation and the smaller internal distance in the fine grain materials.

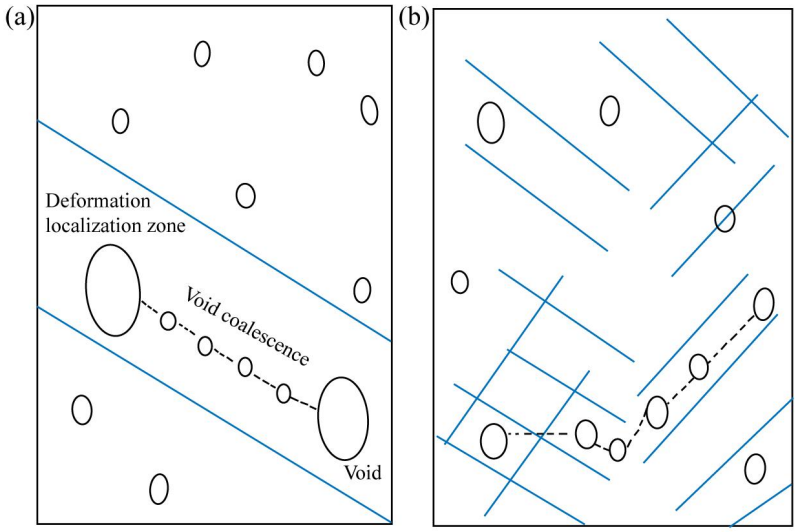

Fig. 20. Schematic showing the coalescence of voids in different grain size conditions: (a) CG, and (b) FG.

Different void coalescence modes result in different morphologies of the fracture surface. The experimental observations in Fig. 7 show a great variation of the morphology of the fracture surface for the samples with different grain sizes. For the FG sample where the microscopic deformation heterogeneity is relatively small, the void growth and coalescence are related to the macroscopic strain and stress state distribution, as shown in Fig. 21(a). During the post-necking deformation, the strain and stress triaxiality in the necking zone., *i.e.*, the central area of the sample, become larger than that in the edge area, and the growth of voids in center region is thus more obviously. The coalescence of voids with similar sizes occurs, which prompts the formation of dimple region in the cup-cone fracture surface. While in the edge area of sample, the growth of void is limited and the coalescence of void is in a shear mode (Besson, 2009a; Torki et al., 2017). With regard to the CG sample in Fig. 21(b), the growth of void is related to the macroscopic as well as the microscopic deformation heterogeneity. Large void also appears at the edge region and the coalescence of very large void finally results in the ductile fracture. This kind of deformation and void evolution facilitates the formation of the fracture surface observed by SEM in Fig. 7(b).

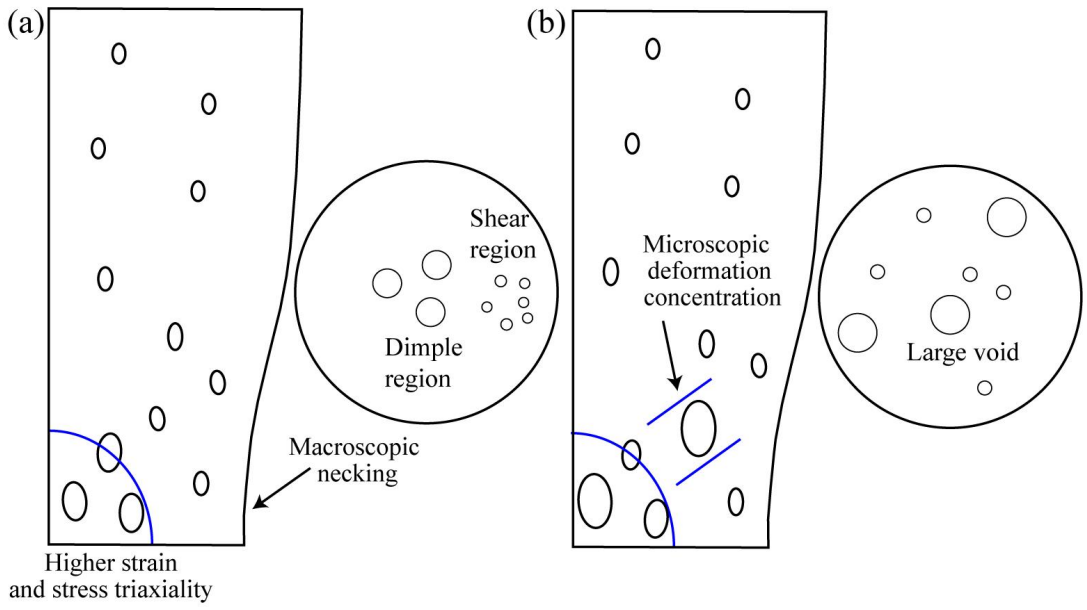

Fig. 21. Schematic showing the deformation distribution, void growth and fracture surface in the uniaxial tensile specimens with different grain sizes: (a) CG, and (b) FG.

3.6 Influence of grain size on ductility

To identify the influence of grain size on the ductility of the material, the simulated void volume fraction (VVF) in RVEs with different grain sizes was examined and presented in Fig. 22. The VVF undergoes a smooth increase during deformation and the average VVF is decreased with grain size. Meanwhile, the standard error of VVF is increased with the grain size. It should be noted that the average value of VVF is not an efficient factor for evaluating the ductility of materials as ductile fracture is more likely to take place in the area with the larger VVF. The experimental elongations of samples possessing different grain sizes are exhibited in Fig. 22. According to the experimental results, a critical VVF of 2.1% was set for the testing material, and the fracture point in simulation is defined as the moment when the largest VVF in the testing RVEs reaches the critical value. The simulated fracture elongation of the RVE is also drawn in Fig. 22. With both the results of experiment and simulation, a fluctuation of ductility is shown for the material in the grain size range of about 40 ~ 300 μm. The ductility is decreased severely when the grain size becomes larger than 300 μm.

The grain size affected ductility is related to the deformation localization caused by the grain structures. When the grain size is small, the deformation heterogeneity is just microscopically, appearing as roughness in the free surface of samples. With the random orientation of grains and the randomly distributed voids, the ductility of materials with only microscopic deformation heterogeneity fluctuates. When the grain size is large enough for inducing macroscopic deformation heterogeneity, such as the experiment result presented in Fig. 22(c) and the simulated result presented in Fig 13(a), the deformation is highly localized in a certain area and the fracture forms in the deformation localization zone at a smaller strain. Ductility thus decreases obviously. Therefore, when the grain size becomes large than the critical value for inducing macroscopic non-uniform deformation, the relationship between

ductility and grain size changes. Apart from large grains, the high extent of mixed grain can also induce macroscopic deformation heterogeneity, and the severe decrease of ductility in experimental results shown in Fig. 22(b) is also related to the mixed grain.

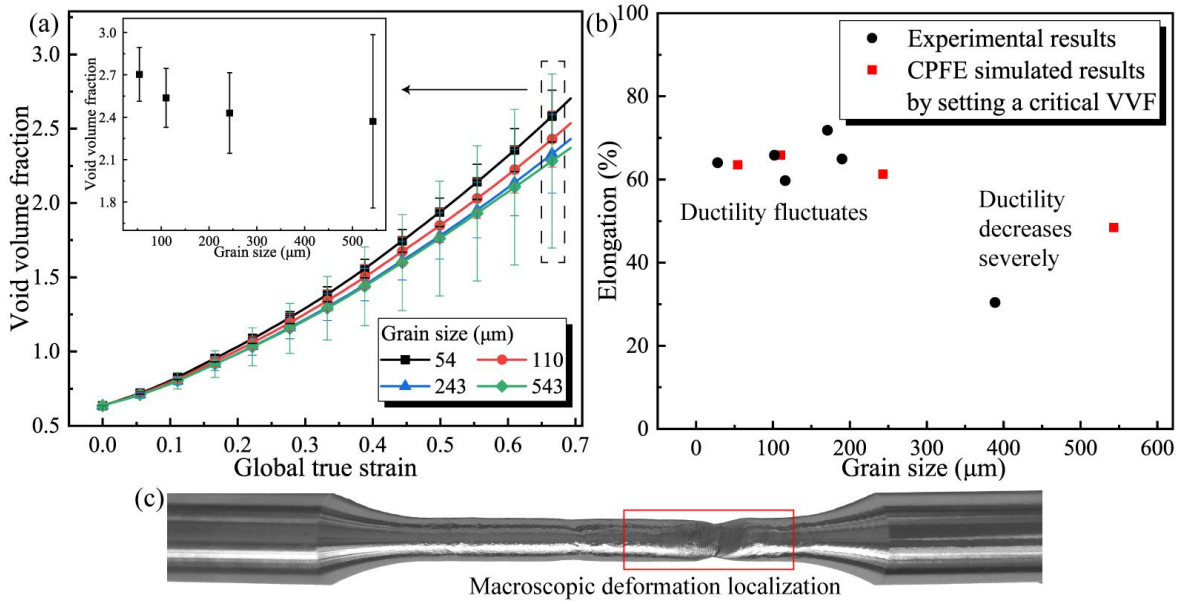

Fig. 22. Influence of grain size on ductility: (a) evolution of void volume fraction for RVE with different grain sizes, (b) relationship between fracture elongation and grain size in experiments and simulations, and (c) macroscopic deformation localization for large and mixed grain sample.

4. Conclusions

Through experimental observations and CPFE simulations of the 316LN steel possessing a random grain orientation, the evolution of void in polycrystalline metals was examined and the influence of grain size on void behavior and ductility was analyzed and identified. The main conclusions drawn in the study are listed in the following:

1. Different morphologies of the fracture surface and free surface of the samples with different grain sizes are observed in experiments, indicating a variation of deformation pattern and void behavior with grain size. The void evolution in plastic deformation was also characterized by experiment, and the evident growth and elongation of void are

observed at the large deformation.

2. According to the CPFE simulation results, the growth of void is related to the non-uniform deformation of polycrystalline material induced by the variation of grain orientation. In deformation concentration zone, the void grows significantly while in small deformation zone, the growth of void is limited.
3. With the increase of grain size, the deformation becomes more heterogeneous and the void size thus becomes more non-uniform. By using the Gaussian function to describe the distribution of major void dimension in the material with a certain grain size, an extended void growth model involving the effect of grain size was established on basis of the Rice and Tracey model.
4. Different types of void coalescence occur in the material with different grain sizes, forming various morphologies of the fracture surface. Very large voids formed in the coarse grain material play an important role on the process of void coalescence.
5. The relationship between grain size and ductility of the testing 316 LN steel was identified. The ductility in the fine grain scenario is not in relation to the grain size but affected by the randomly distributed voids and the microscopic non-uniform deformation. When the grain size is large and the macroscopic deformation localization occurs, the ductility decreases severely as fracture forms earlier in the deformation localization area.

Acknowledgements

The authors gratefully acknowledge the funding support from the National Natural Science Foundation of China with the projects of Nos. 51675335, 51705317 and 51575465. This work is also carried out with the support from Shanghai Sailing Program (Grant No. 17YF1408900) and the project of B-Q55M (152792/16E) from the RGC of Hong Kong Government.

Reference

Abdolvand, H., Majkut, M., Oddershede, J., Wright, J.P., Daymond, M.R., 2015. Study of 3-D stress development in parent and twin pairs of a hexagonal close-packed polycrystal: Part II – crystal plasticity finite element modeling. Acta Mater. 93, 235-245.

Achouri, M., Germain, G., Dal Santo, P., Saidane, D., 2013. Experimental characterization and numerical modeling of micromechanical damage under different stress states. Mater. Des. 50, 207-222.

Alinaghian, Y., Asadi, M., Weck, A., 2014. Effect of pre-strain and work hardening rate on void growth and coalescence in AA5052. Int. J. Plast. 53, 193-205.

Besson, J., 2009a. Continuum Models of Ductile Fracture: A Review. Int. J. Damage Mech. 19, 3-52.

Besson, J., 2009b. Damage of ductile materials deforming under multiple plastic or viscoplastic mechanisms. Int. J. Plast. 25, 2204-2221.

Feng, C., Cui, Z., 2015. A 3-D model for void evolution in viscous materials under large compressive deformation. Int. J. Plast. 74, 192-212.

Fujita, N., Ishikawa, N., Roters, F., Tasan, C.C., Raabe, D., 2018. Experimental–numerical study on strain and stress partitioning in bainitic steels with martensite–austenite constituents. Int. J. Plast. 104, 39-53.

Guery, A., Hild, F., Latourte, F., Roux, S., 2016. Slip activities in polycrystals determined by coupling DIC measurements with crystal plasticity calculations. Int. J. Plast. 81, 249-266.

Gurson, A.L., 1977. Continuum theory of ductile rupture by void nucleation and growth: Part I—Yield criteria and flow rules for porous ductile media. J. Eng. Mater. Technol. 99, 2-15.

Hosokawa, A., Wilkinson, D.S., Kang, J., Maire, E., 2013. Onset of void coalescence in uniaxial tension studied by continuous X-ray tomography. Acta Mater. 61, 1021-1036.

Jia, N., Roters, F., Eisenlohr, P., Kords, C., Raabe, D., 2012. Non-crystallographic shear banding in crystal plasticity FEM simulations: Example of texture evolution in α-brass. Acta Mater. 60, 1099-1115.

Johnson, G.R., Cook, W.H., 1985. Fracture characteristics of three metals subjected to various strains, strain rates, temperatures and pressures. Eng. Frac. Mech. 21, 31-48.

Kadkhodapour, J., Butz, A., Ziaei Rad, S., 2011. Mechanisms of void formation during tensile testing in a commercial, dual-phase steel. Acta Mater. 59, 2575-2588.

Khan, A.S., Liu, H., 2012. Strain rate and temperature dependent fracture criteria for isotropic and anisotropic metals. Int. J. Plast. 37, 1-15.

Kondori, B., Madi, Y., Besson, J., Benzerga, A.A., 2018a. Evolution of the 3D plastic anisotropy of HCP metals: Experiments and modeling. Int. J. Plast.

Kondori, B., Morgeneyer, T.F., Helfen, L., Benzerga, A.A., 2018b. Void growth and coalescence in a magnesium alloy studied by synchrotron radiation laminography. Acta Mater. 155, 80-94.

Landron, C., Bouaziz, O., Maire, E., Adrien, J., 2013. Experimental investigation of void coalescence in a dual phase steel using X-ray tomography. Acta Mater. 61, 6821-6829.

Landron, C., Maire, E., Bouaziz, O., Adrien, J., Lecarme, L., Bareggi, A., 2011. Validation of void growth models using X-ray microtomography characterization of damage in dual phase steels. Acta Mater. 59, 7564-7573.

Lebensohn, R.A., Escobedo, J.P., Cerreta, E.K., Dennis-Koller, D., Bronkhorst, C.A., Bingert, J.F., 2013. Modeling void growth in polycrystalline materials. Acta Mater. 61, 6918-6932.

Li, H., Fu, M.W., Lu, J., Yang, H., 2011. Ductile fracture: Experiments and computations. Int. J. Plast. 27, 147-180.

Li, H., Zhang, H.Q., Yang, H., Fu, M.W., Yang, H., 2017. Anisotropic and asymmetrical yielding and its evolution in plastic deformation: Titanium tubular materials. Int. J. Plast.

90, 177-211.

Lin, Y.C., He, D.-G., Chen, M.-S., Chen, X.-M., Zhao, C.-Y., Ma, X., Long, Z.-L., 2016. EBSD analysis of evolution of dynamic recrystallization grains and δ phase in a nickel-based superalloy during hot compressive deformation. Mater. Des. 97, 13-24.

Lin, Y.C., Yang, H., Xin, Y., Li, C.-Z., 2018. Effects of initial microstructures on serrated flow features and fracture mechanisms of a nickel-based superalloy. Materials Characterization 144, 9-21.

Lou, Y., Chen, L., Clausmeyer, T., Tekkaya, A.E., Yoon, J.W., 2017. Modeling of ductile fracture from shear to balanced biaxial tension for sheet metals. Int. J. Solids Struct. 112, 169-184.

Lou, Y., Huh, H., Lim, S., Pack, K., 2012. New ductile fracture criterion for prediction of fracture forming limit diagrams of sheet metals. Int. J. Solids Struct. 49, 3605-3615.

Morgeneyer, T.F., Taillandier-Thomas, T., Helfen, L., Baumbach, T., Sinclair, I., Roux, S., Hild, F., 2014. In situ 3-D observation of early strain localization during failure of thin Al alloy (2198) sheet. Acta Mater. 69, 78-91.

Nahshon, K., Hutchinson, J.W., 2008. Modification of the Gurson Model for shear failure. Eur. J. Mech. A 27, 1-17.

Nemcko, M.J., Qiao, H., Wu, P., Wilkinson, D.S., 2016. Effects of void fraction on void growth and linkage in commercially pure magnesium. Acta Mater. 113, 68-80.

Noell, P., Carroll, J., Hattar, K., Clark, B., Boyce, B., 2017. Do voids nucleate at grain boundaries during ductile rupture? Acta Mater. 137, 103-114.

Novella, M.F., Ghiotti, A., Bruschi, S., Bariani, P.F., 2015. Ductile damage modeling at elevated temperature applied to the cross wedge rolling of AA6082-T6 bars. J. Mater. Process. Technol. 222, 259-267.

Pardoen, T., Hutchinson, J.W., 2000. An extended model for void growth and coalescence. J.

Mech. Phys. Solids 48, 2467-2512.

Raabe, D., Ma, D., Roters, F., 2007. Effects of initial orientation, sample geometry and friction on anisotropy and crystallographic orientation changes in single crystal microcompression deformation: A crystal plasticity finite element study. Acta Mater. 55, 4567-4583.

Rice, J.R., Tracey, D.M., 1969. On the ductile enlargement of voids in triaxial stress fields∗. J. Mech. Phys. Solids 17, 201-217.

Sachtleber, M., Zhao, Z., Raabe, D., 2002. Experimental investigation of plastic grain interaction. Mater. Sci. Eng. A 336, 81-87.

Scott, H., Boyd, J.D., Pilkey, A.K., 2017. Micro-computed tomographic imaging of void damage in a hot-rolled complex phase sheet steel. Mater. Sci. Eng. A 682, 139-146.

Selvarajou, B., Joshi, S.P., Benzerga, A.A., 2019. Void growth and coalescence in hexagonal close packed crystals. J. Mech. Phys. Solids 125, 198-224.

Shang, X., Cui, Z., Fu, M.W., 2017. Dynamic recrystallization based ductile fracture modeling in hot working of metallic materials. Int. J. Plast. 95, 105-122.

Shang, X., Cui, Z., Fu, M.W., 2018. A ductile fracture model considering stress state and Zener–Hollomon parameter for hot deformation of metallic materials. Int. J. Mech. Sci. 144, 800-812.

Sun, C.Y., Guo, N., Fu, M.W., Wang, S.W., 2016. Modeling of slip, twinning and transformation induced plastic deformation for TWIP steel based on crystal plasticity. Int. J. Plast. 76, 186-212.

Tang, X.F., Peng, L.F., Shi, S.Q., Fu, M.W., 2019. Influence of crystal structure on size dependent deformation behavior and strain heterogeneity in micro-scale deformation. Int. J. Plast. 118, 147-172.

Taylor, K.L., Sherry, A.H., 2012. The characterization and interpretation of ductile fracture

mechanisms in AL2024-T351 using X-ray and focused ion beam tomography. Acta Mater. 60, 1300-1310.

Thomason, P.F., 1985a. A three-dimensional model for ductile fracture by the growth and coalescence of microvoids. Acta Metall. 33, 1087-1095.

Thomason, P.F., 1985b. Three-dimensional models for the plastic limit-loads at incipient failure of the intervoid matrix in ductile porous solids. Acta Metall. 33, 1079-1085.

Torki, M.E., 2019. A unified criterion for void growth and coalescence under combined tension and shear. Int. J. Plast.

Torki, M.E., Tekoğlu, C., Leblond, J.B., Benzerga, A.A., 2017. Theoretical and numerical analysis of void coalescence in porous ductile solids under arbitrary loadings. Int. J. Plast. 91, 160-181.

Tvergaard, V., 1981. Influence of voids on shear band instabilities under plane strain conditions. Int. J. Fract. 17, 389-407.

Tvergaard, V., Needleman, A., 1984. Analysis of the cup-cone fracture in a round tensile bar. Acta Metall. 32, 157-169.

Ueda, T., Helfen, L., Morgeneyer, T.F., 2014. In situ laminography study of three-dimensional individual void shape evolution at crack initiation and comparison with Gurson–Tvergaard–Needleman-type simulations. Acta Mater. 78, 254-270.

Weck, A., Wilkinson, D.S., 2008. Experimental investigation of void coalescence in metallic sheets containing laser drilled holes. Acta Mater. 56, 1774-1784.

Weck, A., Wilkinson, D.S., Maire, E., Toda, H., 2008. Visualization by X-ray tomography of void growth and coalescence leading to fracture in model materials. Acta Mater. 56, 2919-2928.

Yang, C., Liu, H., Yang, B., Shi, B., Peng, Y., Pan, F., Wu, L., 2019. The effect of pre-twinning on the mechanical behavior of free-end torsion for an extruded AZ31

magnesium alloy. Mater. Sci. Eng. A 743, 391-396.

Yang, C., Shi, B., Peng, Y., Pan, F., 2018. Transition from convex to concave of equal plastic work contours for wrought magnesium alloy under multi-axial loading. Int. J. Solids Struct. 150, 117-124.

Zhang, H., Dong, X., Wang, Q., Zeng, Z., 2012. An effective semi-implicit integration scheme for rate dependent crystal plasticity using explicit finite element codes. Comp. Mater. Sci. 54, 208-218.

Zhang, H., Liu, J., Sui, D., Cui, Z., Fu, M.W., 2018. Study of microstructural grain and geometric size effects on plastic heterogeneities at grain-level by using crystal plasticity modeling with high-fidelity representative microstructures. Int. J. Plast. 100, 69-89.